Paleocurrent reconstruction of the deep Pacific inflow during the middle Miocene: Reflections of East Antarctic Ice Sheet growth

Ian R. Hall,[1] I. Nicholas McCave,[2] Rainer Zahn,[1,3] Lionel Carter,[4] Paul C. Knutz,[1,2,5] and Graham P. Weedon[6]

Received 12 June 2002; revised 10 December 2002; accepted 7 February 2003; published 22 May 2003.

[1] Today the deep western boundary current (DWBC) east of New Zealand is the most important route for deep water entering the Pacific Ocean. Large-scale changes in deep water circulation patterns are thought to have been associated with the development of the East Antarctic Ice Sheet (EAIS) close to the main source of bottom water for the DWBC. Here we reconstruct the changing speed of the southwest Pacific DWBC during the middle Miocene from ~15.5–12.5 Ma, a period of significant global ice accumulation associated with EAIS growth. Sortable silt mean grain sizes from Ocean Drilling Program Site 1123 reveal variability in the speed of the Pacific inflow on the timescale of the 41 kyr orbital obliquity cycle. Similar orbital period flow changes have recently been demonstrated for the Pleistocene epoch. Collectively, these observations suggest that a strong coupling between changes in the speed of the deep Pacific inflow and high-latitude climate forcing may have been a persistent feature of the global thermohaline circulation system for at least the past 15 Myr. Furthermore, long-term changes in flow speed suggest an intensification of the DWBC under an inferred increase in Southern Component Water production. This occurred at the same time as decreasing Tethyan outflow and major EAIS growth between ~15.5 and 13.5 Ma. These results provide evidence that a major component of the deep thermohaline circulation was associated with the middle Miocene growth of the EAIS and support the view that this time interval represents an important step in the development of the Neogene icehouse climate. *INDEX TERMS:* 1615 Global Change: Biogeochemical processes (4805); 1635 Global Change: Oceans (4203); 1694 Global Change: Instruments and techniques; *KEYWORDS:* Miocene, deep western boundary current, sortable silt, sediment drifts, Ocean Drilling Program, southwest Pacific

Citation: Hall, I. R., I. N. McCave, R. Zahn, L. Carter, P. C. Knutz, and G. P. Weedon, Paleocurrent reconstruction of the deep Pacific inflow during the middle Miocene: Reflections of East Antarctic Ice Sheet growth, *Paleoceanography*, *18*(2), 1040, doi:10.1029/2002PA000817, 2003.

1. Introduction

[2] The abyssal circulation of waters originating in the Southern Ocean is an important control in Earth's heat budget. As much as 55–60% of the oceanic volume is cooled around Antarctica [*Gordon*, 1988] and today, some 35–40% of the flux of bottom water entering the major ocean basins does so through the southwest Pacific gateway [*Warren*, 1981; *Schmitz*, 1995] constituted by the prominent western boundary of the New Zealand plateau, including Chatham Rise, the location of Ocean Drilling Program Site 1123 (Figure 1). During its passage through the gateway, the abyssal flow receives an influx of terrigenous detritus mainly derived from the rapidly rising mountains along the New Zealand sector of the Australian-Pacific plate boundary [*Carter et al.*, 1996]. Near Chatham Rise, the flow passes beneath the productive surface waters associated with the Subtropical Front. The terrigenous influx, together with pelagic biogenic sediment, has been transported and deposited by the abyssal flow to form a series of prominent drifts distributed along the New Zealand margin [*Carter and McCave*, 1994; *McCave and Carter*, 1997].

[3] The present abyssal circulation past New Zealand is a composite feature. North of ~49°S, it is dominated by the thermohaline deep western boundary current (DWBC). With an average volume transport of 16 ± 11.9 Sv (1 Sv = 10^6 m^3 s^{-1}) at 32°30′S [*Whitworth et al.*, 1999], this is the largest water flux in a DWBC in the world ocean. Further south, the Antarctic Circumpolar Current (ACC) travels northeastward along the flank of Campbell Plateau. The wind-driven but deep-reaching ACC appears to interact with the underlying thermohaline DWBC as shown by modeling studies which suggest that the ACC affects the underlying deep water flow through eddy coupling [*Carter*

[1]Department of Earth Sciences, Cardiff University, Cardiff, UK.
[2]Department of Earth Sciences, University of Cambridge, Cambridge, UK.
[3]Institució Catalana de Recerca i Estudis Avançats, Grup de Recerca Consolidat en Geociències Marines, Facultat de Geologia, Universitat de Barcelona, Barcelona, Spain.
[4]National Institute of Water and Atmosphere, Kilbirnie, Wellington, New Zealand.
[5]Geological Institute, University of Copenhagen, Copenhagen, Denmark.
[6]Centre for Environmental Change and Volcanic Studies, University of Luton, Luton, UK.

Copyright 2003 by the American Geophysical Union.
0883-8305/03/2002PA000817

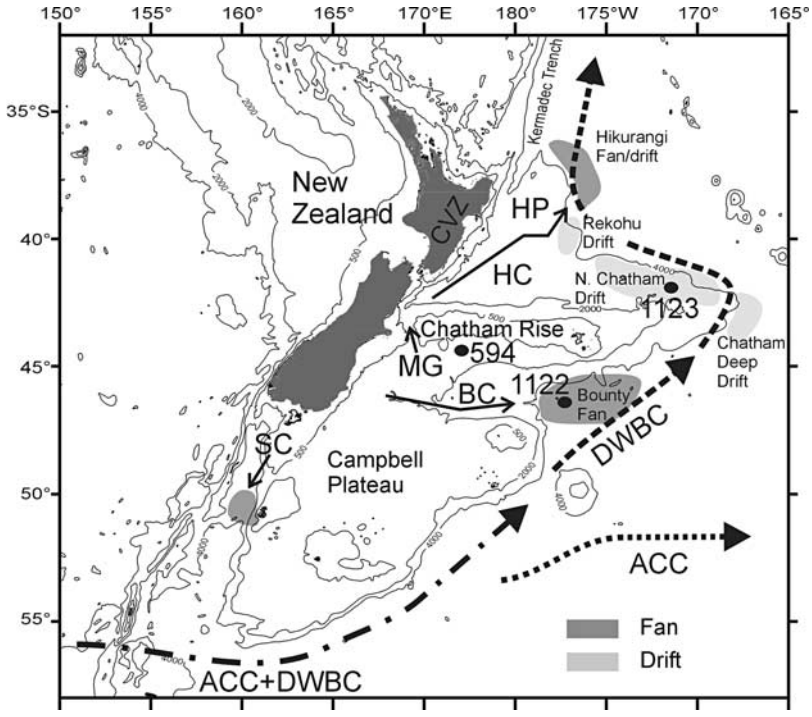

Figure 1. Location of study area with a generalized abyssal circulation scheme, sediment fans, and drifts, which together make up the major elements of the Eastern New Zealand Oceanic Sedimentary System (ENZOSS after *Carter et al.* [1996]). Also shown are the locations of ODP Sites 1122 and 1123 and DSDP Site 594. Contours are at 500, 2000, and 4000 m. Abbreviations are: ACC, Antarctic Circumpolar Current; DWBC, Deep Western Boundary Current; CVZ, Central Volcanic Zone; HP, Hikurangi Plateau; MG, Mernoo Gap; SC, Solander Channel; BC, Bounty Channel; and HC, HiKurangi Channel.

and Wilkin, 1999; *Morrow et al.*, 1992]. The regional distribution of abyssal eddy kinetic energy with values up to 80 $cm^2\ s^{-2}$ along the flank of Campbell Plateau compared to <1–2 $cm^2\ s^{-2}$ north of the Chatham Rise [*Carter and Wilkin*, 1999; *Hollister and McCave*, 1984] point to ACC domination over the abyssal flow in the southern part of the gateway. Indeed, this contention is supported by observations of intense erosion along the base of Campbell Plateau but quiescent conditions further north where the DWBC prevails [*McCave and Carter*, 1997].

[4] The dominant water mass carried by the modern DWBC is Circumpolar Deep Water (CDW) which has three main components [*Warren*, 1973, 1981; *McCave and Carter*, 1997; *Whitworth et al.*, 1999]: upper CDW, a strongly nutrient-enriched and oxygen-depleted layer located between 1400 and 2800 m water depth; middle CDW, a distinct high-salinity (S = 34.72–34.73) core layer between 2800 and 3800 m, including the zone of maximum influence of North Atlantic Deep Water (2800–3400 m); and lower CDW (LCDW), a cold, but lower salinity (S = 34.68) layer >3800 m water depth. The LCDW is largely generated around Antarctica, in particular by cold water formed in the Weddell Sea, near the Adelie Coast and probably by water from the Ross Sea (i.e., in a broad sense Antarctic Bottom Water, AABW of former usage) [*Orsi et al.*, 1999].

[5] During the middle Miocene, global climate cooled significantly [*Shackleton and Kennett*, 1975; *Woodruff and Savin*, 1989; *Flower and Kennett*, 1993, 1994]. At about 15 Ma ago $\delta^{18}O$ isotopic records suggest that there was rapid growth of the East Antarctic Ice Sheet (EAIS) to something like its present size [*Shackleton and Kennett*, 1975; *Kennett*, 1977; *Loutit et al.*, 1983; *Miller and Katz*, 1987; *Miller et al.*, 1991; *Wright et al.*, 1992; *Wright and Miller*, 1993; *Flower and Kennett*, 1993; *Barrett*, 1996]. This had impacts on the deep circulation in the period 16.5–13.8 Ma tracked by carbon isotope measurements of foraminifera from the Tasman Sea west of New Zealand [*Flower and Kennett*, 1995]. Three water masses are involved, warm Northern Component Water (NCW), Tethyan Indian Saline Water (TISW) and cold, Southern Component Water (SCW). As Antarctica cooled TISW decreased in magnitude and production of the SCW increased. This led to intensified bottom currents that may have produced an erosional hiatus at some localities [*Sykes et al.*, 1998; *Ramsay et al.*, 1998].

[6] In this paper, we assess the behavior of the deep inflow to the southwest Pacific over the period ~15.5–12.5 Ma. Moreover, we examine the evidence for orbital forcing of the DWBC speed proxy. This proxy may be directly related to the climatically forced fluctuations in production of SCW, i.e., equivalent to modern AABW, that are superimposed on the middle Miocene decline in global temperature and the expansion of global ice volume.

2. Paleocurrent Proxy: Sortable Silt Mean Grain Size

[7] Attempts to correlate grain size to relative paleocurrent intensity were first made during the mid-seventies

[*Ledbetter and Johnson*, 1976]. Since that time, improvements in both understanding of the dynamic processes of erosion, sorting and deposition of muds [*McCave*, 1984] and analytical capability [*Syvitski*, 1991; *Bianchi et al.*, 1999] have led to the development of the sortable silt mean size ($\overline{SS}$); the mean grain size of the 10–63 μm terrigenous fraction, with biogenic carbonate and opal removed [*McCave et al.*, 1995]. *McCave et al.* [1995] showed that the fine end of the silt fraction (<10 μm equivalent spherical diameter) is normally cohesive in nature and deposited mainly as aggregates together with clay. Therefore the size spectrum of such disaggregated fine material cannot reflect the fluid shear of the depositional environment. The mean size of the >10 μm silt, which mainly behaves noncohesively during transport and deposition, is an indicator of flow speed. The $\overline{SS}$ is a parameter whose coarser values reflects stronger near-bottom flow and selective deposition and winnowing. The proxy indicates relative current speed but is presently uncalibrated in terms of velocity. Some idea of actual current speed can be gained by comparison with critical erosion and deposition curves [*McCave et al.*, 1995]. To minimize source effects, the sediment should be transported in several sorting operations to the site of deposition by the current whose properties are being inferred. The initial terrigenous material should contain the full range of sizes in the 10–63 μm range, and not vary strongly over the period of interest. The $\overline{SS}$ proxy has given results consistent with other paleohydrographic proxies in a number of studies [e.g., *Hall et al.*, 1998, 2001; *Bianchi et al.*, 2001], and similarity of behavior of this parameter at separated sites in the Atlantic deep circulation system has strengthened confidence in its ability to reveal regional flow changes without local short-term interference [*Hall et al.*, 1998].

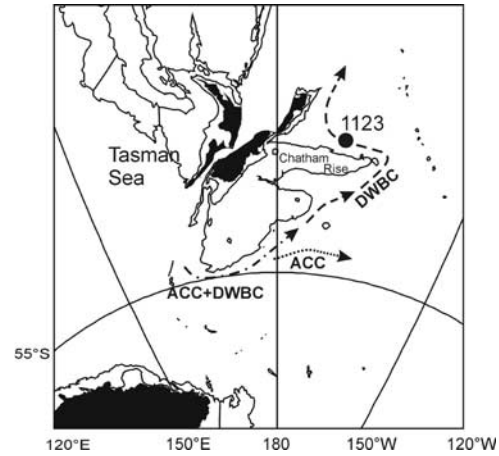

Figure 2. Middle Miocene paleogeographic reconstruction of the study area for 15 Ma showing location of Site 1123. A generalized ancestral abyssal circulation scheme is included. Chatham Rise was at least as shallow in the middle Miocene as at present and possibly shallower. We suggest that the 1000 km-long high formed a barrier that would have confined the paleo-ACC to its south side; i.e., it would have been the northern limit of the Subantarctic Front in the same way that in the Quaternary it appears to have formed a fixed locus of the subtropical convergence [*Weaver et al.*, 1997]. If this were the case then it is likely that the ACC uncoupled from the DWBC in a similar region as at present (Figure 1) and therefore the ACC did not directly impinge upon Site 1123. Abbreviations are: ACC, Antarctic Circumpolar Current and DWBC, Deep Western Boundary Current. (Map courtesy of A. Smith, Cambridge Palaeomap Services, Department of Earth Sciences, Cambridge, UK).

3. Site Information

[8] Ocean Drilling Program Site 1123 (41° 47.2′S, 171° 29.9′W) is located 410 km northeast of the Chatham Islands, on the northeastern flank of Chatham Rise, in a water depth of 3290 m. The cores were obtained from the extensive North Chatham Drift that is deposited as the DWBC decelerates after passing through Valerie Passage that separates Chatham Rise from Louisville Seamount Chain. Thus the site is well placed to monitor the deep Pacific inflow. The drift is around 550 km in length and ranges in water depths between 2200 and 4500 m (Figure 1). Seismic sections show that the drift is >1000 m (>1.0 s two-way travel time) thick at water depths less than 3500 m [*Carter and McCave*, 1994]. The stratigraphic sequence is remarkably uniform above ~465 m composite depth (mcd) being primarily nannofossil ooze and chalk with varying amounts of terrigenous mud [*Carter et al.*, 1999a].

[9] The paleogeography of the southern Indo-Pacific region in the middle Miocene (Figure 2) shows that the configuration of oceanic topography was broadly similar to the present. The Tasman Sea, in which seafloor-spreading ceased at 52 Ma [*Gaina et al.*, 1998], formed a circulation dead-end below about 2000 m water depth as at present, and would not have provided a route for cold deep water to enter the Pacific from the south. At present, the Campbell Plateau, the Chatham Rise and the Hikurangi Plateau provide the effective western boundary to the ocean over nearly 18° of latitude (note that the boundary is between 56° and ~38°S) (Figure 1). During the middle Miocene, Chatham Rise was ~2° south of its present position [*Sclater et al.*, 1985]. It is thus most probable that, with a source of dense water to the south, under the Stommel-Aarons model [e.g., *Stommel*, 1958], a DWBC flowed then, as now, to the north along this margin. This is supported by the presence of displaced sub-Antarctic diatoms, which are inferred to have been entrained into the sediments by the DWBC (i.e., CDW) throughout the late Miocene to Pleistocene [*Carter et al.*, 1999a]. The paleowater depth of Site 1123 may be assessed from the geology of Chatham Rise. Upper Eocene shelly limestone of shallow marine origin and disconformably overlying Mio-Pliocene shallow submarine volcanics with some shallow marine pectenid fossils are exposed on the Chatham Islands. Seabed samples west of the Chatham Islands also contain limestone and basalt of early Miocene age indicating stability of a shallow marine environment on the crest of Chatham Rise through the mid-Tertiary [*Cullen*, 1965]. We estimate the paleowater depth of Site 1123 in the early-middle Miocene to have been very similar to today, certainly not deeper and no more than a few hundred meters shallower. Sedimentation rates (*Carter et al.* [1999a] and

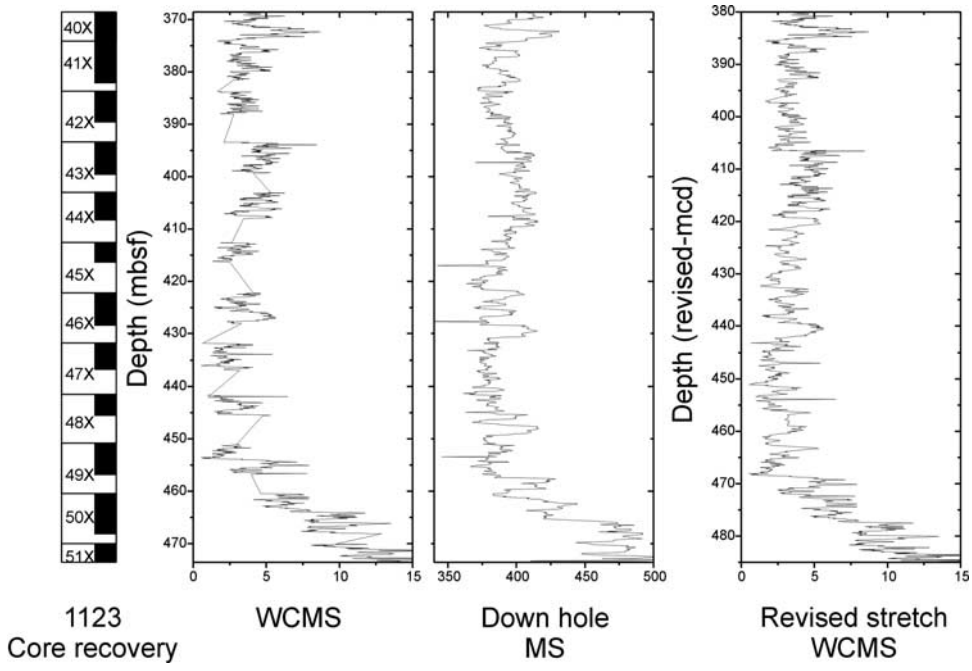

Figure 3. Comparison of the whole core magnetic susceptibility (WCMS) with nonlinear stretched WCMS and the down-hole log susceptibility record. Key features in the WCMS record were tied to presumed equivalent features in the down-hole MS log. The WCMS records were then stretched linearly between the tie points. This improved the match between the stretched WCMS record and the down-hole MS log and provided a revised meters composite depth (rmcd) depth scale (Figure 3). Also shown is the core recovery. Data from *Carter et al.* [1999a].

those presented here) together with the sedimentary architecture [*Carter and McCave*, 1994] indicate that Site 1123 was a drift sequence in the middle Miocene.

4. Pleistocene Paleocurrent Reconstruction at Site 1123

[10] Using sedimentological and geochemical records from Site 1123, *Hall et al.* [2001] demonstrated an intensification of the DWBC flow, and Pacific deep-water ventilation, during glacial periods over the past 1.2 million years. Their sortable silt mean grain size record showed significant spectral peaks at each of the orbital frequencies, which were coherent with benthic records of both oxygen and carbon isotopes at 98% (for 100 and 41 ka) and 90% confidence (for 23 ka). *Hall et al.* [2001] suggest that the pattern of increased glacial DWBC flow speeds was related to greater glacial production of AABW, a feature supported by the diatom tracer data of *Stickley et al.* [2001]. These results resolved the paradox that, although the DWBC has a very large flux, presently it appears to be slow-moving around the New Zealand Margin (shown by current meters, nepheloid layers, bottom photographs), yet there are extensive scours around volcanic pinnacles on the seabed [*McCave and Carter*, 1997] because the flux was greater in the past. In addition, further downstream, these enhanced flows may have produced the circulation changes that drove the glacial increase in sediment focusing recorded in the central equatorial Pacific over the past 300 kyr [*Marcantonio et al.*, 2001]. At present little is known regarding the early geological record, or history of the variability in the vigor, of the deep Pacific inflow.

5. Methods

[11] We have sampled the gradual cooling period (~15.5 to 12.5 Ma) that is believed to mark the reestablishment of a major ice sheet on Antarctica following the late middle Miocene climatic optimum [e.g., *Flower and Kennett*, 1994]. Sediment samples of 10 cm^3 were taken at ~5–10 cm intervals (approximating a temporal spacing between samples of 1–10 kyr). The sampling interval was between 181-1123B-45X-1, 3–5 cm and 181-1123B-51X-1, 144–145 cm (412.63–471.44 m below seafloor, mbsf). Recovery (meters of core relative to meters advanced by the drill string) in XCB cores 181-1123B-45X to 50X, was moderate (<70%). The samples for this sequence were assigned revised meters composite depths (rmcd) by tying the whole core magnetic susceptibility record to the down-hole magnetic susceptibility log (Figure 3).

[12] Samples were initially disaggregated in 0.2% *Calgon* on a rotating carousel for a period of 48 hours. Each sample was then washed over a 63 μm sieve. Examination of the coarse fraction confirmed that foraminiferal tests were too diagenetically altered for isotopic analysis. Carbonate contents were estimated from the determination of inorganic carbon by instrumental CHN analyses. Measurements of magnetic susceptibility were made on the <63 μm fraction

using a Bartington MS2B sensor.

[13] To derive $\overline{SS}$, grain size distributions of the fine terrigenous fraction were determined using a Micromeritics SediGraph 5100, following removal of carbonate, by dissolution in 1 M acetic acid solution (48h at room temperature), and biogenic opal, by digestion in 2 M sodium carbonate solution (85°C for 5 h). Analytical precision ranged between ±1.5–6.0% (or ±0.02-0.9 μm at 15 μm) depending on the percentage of 10–63 μm material in a sample [*Bianchi et al.*, 1999].

[14] There is some potential uncertainty in assessing the significance of the $\overline{SS}$ parameter in regions of high eddy kinetic energy (K_E). However, Site 1123 lies at a location where estimates of modern benthic K_E are <1–2 cm^2 s^{-2}, well north of the energetic ACC. Thus mean flow rather than the eddy flow is expected to dominate the $\overline{SS}$ signal if the Miocene flow was the thermohaline DWBC. We have a good understanding of the contemporary DWBC as it operates within the Eastern New Zealand Oceanic Sedimentary System (ENZOSS) and of the sediment supply to Site 1123 [*Carter et al.*, 1996; *Hall et al.*, 2002]. The mass accumulation of terrigenous sediment at Site 1123 varies on glacial-interglacial timescales during the Pleistocene [*Hall et al.*, 2002]. Nevertheless, this terrigenous material remains size sorted under the influence of the DWBC [*Hall et al.*, 2001]. The likelihood of a significant cyclical change in the characteristics of the terrigenious sediment supply to Site 1123 was probably less during the middle Miocene. This is because the major terrigenous sediment pathway, via the Bounty Channel, presently some 1300 km to the south of Site 1123, was yet to be established [*Hall et al.*, 2002]. Also, the hemipelagic supply from this region is liable to have been extremely small judging by the predominance of calcareous biopelagites at Deep Sea Drilling Project (DSDP) Site 594 (Figure 1) up to the early Pliocene [*Nelson et al.*, 1986]. Accordingly we can satisfy the general prerequisites associated with the paleocurrent interpretation of the $\overline{SS}$ parameter [*McCave et al.*, 1995; *Bianchi et al.*, 1999].

[15] Power spectra were calculated using the Lomb-Scargle algorithm for irregularly spaced data [*Press et al.*, 1992]. Spectral smoothing used three applications of a discrete Hanning window, yielding eight degrees of freedom. Spectral confidence levels were located using the robust AR(1) modeling of median-smoothed spectra [*Mann and Lees*, 1996]. Filtering and tuning were performed using Analyseries 1.1 [*Paillard et al.*, 1996].

6. Results and Discussion

6.1. Stratigraphy and Orbital Control on DWBC Flow Speeds

[16] The sedimentological parameters shown against rmcd in Figure 4 are characterized by high-frequency cyclic variations as well as long-term gradual changes in properties. Carbonate concentrations range between 20 and 80 wt% (Figure 4a). The lower interval between 484 and 465 rmcd displays a progressive increase in calcium carbonate punctuated by spikes of lower calcium carbonate content. Magnetic susceptibility (Figure 4b) shows a clear inverse relationship to calcium carbonate. A similar trend in the silt/clay ratio suggests that the increase in calcium carbonate content corresponds to an increase in the silt abundance (Figure 4c). Sortable silt mean grain sizes range between 12 and 19 μm (Figure 4d) similar to the Pleistocene section of Site 1123 [*Hall et al.*, 2001]. Following the minimum in $\overline{SS}$ at around 478 rmcd, values increase and suggest an intensification of the DWBC flow at that time.

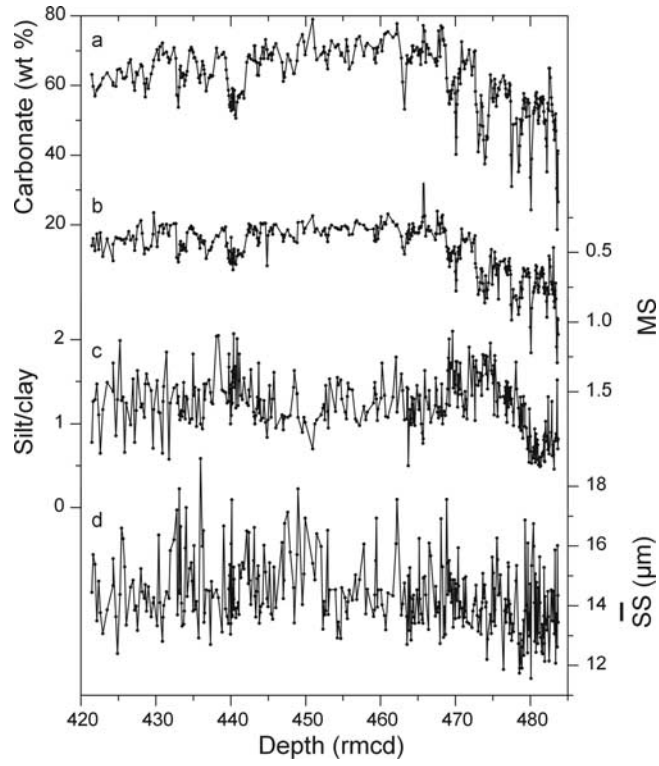

Figure 4. Sedimentological data for Site 1123 versus depth (rmcd). Shown are records of (a) calcium carbonate, (b) magnetic susceptibility (note reversed scale), (c) silt/clay ratio, and (d) $\overline{SS}$.

[17] Although complicated by poor recovery in the lowermost interval of Hole 1123B, the magnetic polarity record from Site 1123 is extremely comprehensive (16 events during 15.5–12.5 Ma) with all known reversals present back to about 15 Ma [*Carter et al.*, 1999a]. The middle Miocene interval at Site 1123 is also well constrained by key foraminiferal, nannofossil and diatom datum levels [*Carter et al.*, 1999a]. In summary: (1) a thick interval of reversed polarity between 499 and 482 rmcd containing the foraminiferal evolutionary transition of *G. miozea* to *G. praemenardii* dated in New Zealand at ~15.8 Ma [*Scott*, 1979; *Morgans et al.*, 1996] is correlated with C5Br; (2) the last occurrence of the nannofossil *Sphenolithus heteromorphus* (13.52 Ma) at ~463 rmcd suggests that the normal polarity events between ~482 and 457 rmcd correlate with Chrons C5ADn, C5ACn, C5ABn and Subchrons C5Bn.2n and C5Bn.1n; (3) the foraminiferal evolutionary transition of *G. praemenardii* to *G. miotumida* (~13.2 Ma) between ~453 and 443 rmcd suggests that the normal polarity events in this interval correlate with Chron C5AAn, and Subchrons C5Ar.2n and Chron C5Ar.1n respectively. Nonetheless,

importantly, shipboard biostratigraphy suggests the possibility of a hiatus between 15 and 14 Ma [*Carter et al.*, 1999a].

[18] In order to investigate the possibility of a hiatus within the 15–14 Ma section and to test an indirect orbital control on a major limb of the deep ocean circulation during that time we have attempted an astronomical calibration using the time series shown in Figure 4. As a tuning target we used the orbital obliquity history calculated from the orbital solution of *Laskar et al.* [1993]. It should be noted that we have not imposed a time lag on the orbital obliquity history for the purposes of our age model as we have no tight control on such lags in the Miocene world with a largely ice-free Northern Hemisphere. As a tuning variable $\overline{SS}$ values were utilized. Other variables considered for tuning were calcium carbonate, MS and light reflectance. However, calcium carbonate contents and MS measured on core samples, though inversely related to each other, are characterized by a much lower-frequency signal that apparently excludes significant obliquity-scale oscillations. The reflectance signal contains considerable high-frequency variability. Unfortunately, in this part of the Site 1123 cores, the reflectance record appears to be largely noise probably related to automated measurement that included, as well as intact biscuits, fractures and the deformed sediment slurry between biscuits. In the depth domain reflectance shows no obvious concentration of variance at a particular wavelength (unlike $\overline{SS}$) and tuning of reflectance to obliquity failed to produce a convincing concentration of variance at the orbital frequencies.

[19] Spectral analysis of the fluctuation in $\overline{SS}$ in the depth domain revealed dominant cycles with a wavelength of about 1.11 m over the entire sequence (Figure 5a). The Pleistocene record of *Hall et al.* [2001] clearly indicates that $\overline{SS}$ maxima correlate with glacial conditions, and $\overline{SS}$ is coherent with benthic $\delta^{18}O$ at periods of 100, 41 and 23 kyr. $\overline{SS}$ and benthic $\delta^{18}O$ are in phase at the 100 kyr period, but lead $\delta^{18}O$ by 2.1 ±1.4 kyr at the 41 kyr period.

[20] We have therefore tuned $\overline{SS}$ maxima (broadly equivalent to calcium carbonate minima as in the Pleistocene series: see below) to the orbital obliquity minima, assuming no phase difference. The assumption of zero phase differences may be an oversimplification of the actual phase relationship between the $\overline{SS}$ and the insolation record, but the lag of the Pleistocene data for the 41 kyr period suggests any error is probably small. The magnetostratigraphy [*Carter et al.*, 1999a] based on the Geomagnetic Polarity Timescale (GPTS) [*Cande and Kent*, 1995; *Berggren et al.*, 1995a, 1995b] was used for initial time markers and the $\overline{SS}$ record was correlated to the inverted obliquity history. Initially, this approach was made working from the top of the record downward and then from bottom up. The results of this tuning identified a section of extremely low sedimentation rates at ~470 rmcd and a lack of cycles within the $\overline{SS}$ record to accommodate the magnetostratigraphy. We therefore suggest the presence of an unconformity somewhere within the normal polarity event, Chron C5ADn (14.612–14.178 Ma on the GPTS). At Site 1123 a short reversed polarity interval, which is not found in the GPTS, separates Chron C5ADn into two normal polarity events. The exact location of the unconformity within C5ADn cannot be determined yet. We have therefore arbitrarily placed the base of the unconformity at the base of C5ADn and then continued the mapping of the $\overline{SS}$ maxima to obliquity minima down the record. This locates the unconformity between ~475.30–475.42 rmcd and represents a time gap of ~300 kyr (14.612–14.318 Ma). This choice of location for the unconformity produces the closest fit to the GPTS of *Berggren et al.* [1995b]. After tuning (Figure 6), the $\overline{SS}$ record was band pass filtered in the time domain around the frequency of the resulting spectral peak

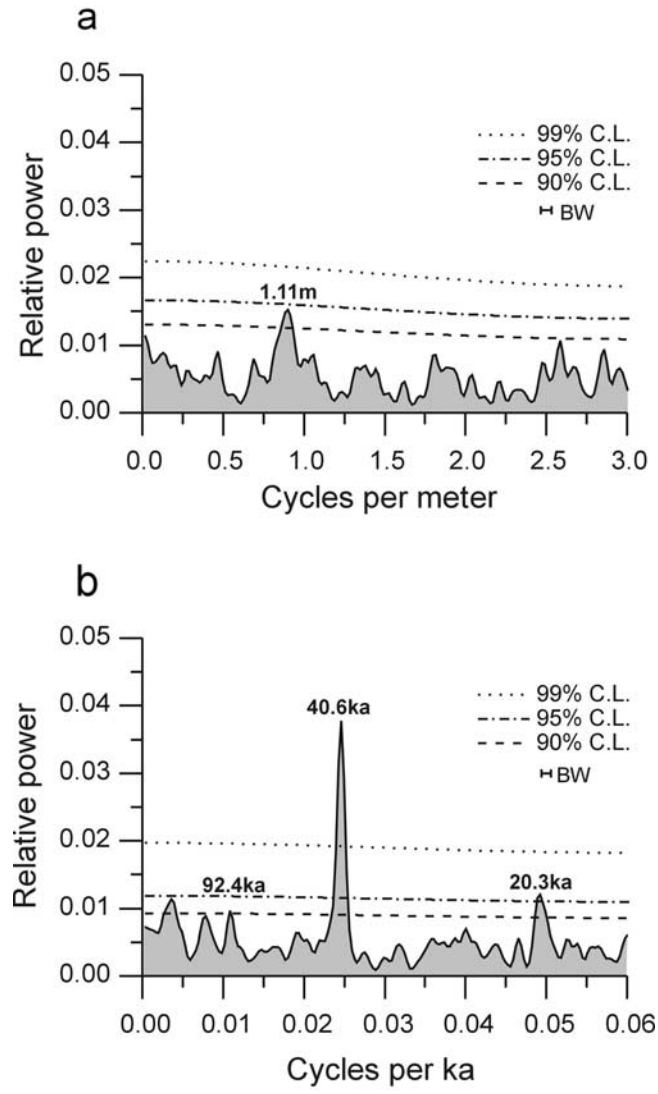

Figure 5. Power spectra of $\overline{SS}$ for the whole record in (a) depth (rmcd) and (b) in age following tuning. Abbreviations are: BW, bandwidth; C. L., confidence level. Note: the significant spectral peak corresponding to a period of 92.4 kyr might be associated with orbital eccentricity. On the other hand the significant spectral peak corresponding to a period of 20.3 kyr is probably a second harmonic of the orbital obliquity peak (period 40.6 kyr) rather than an indication of orbital precession.

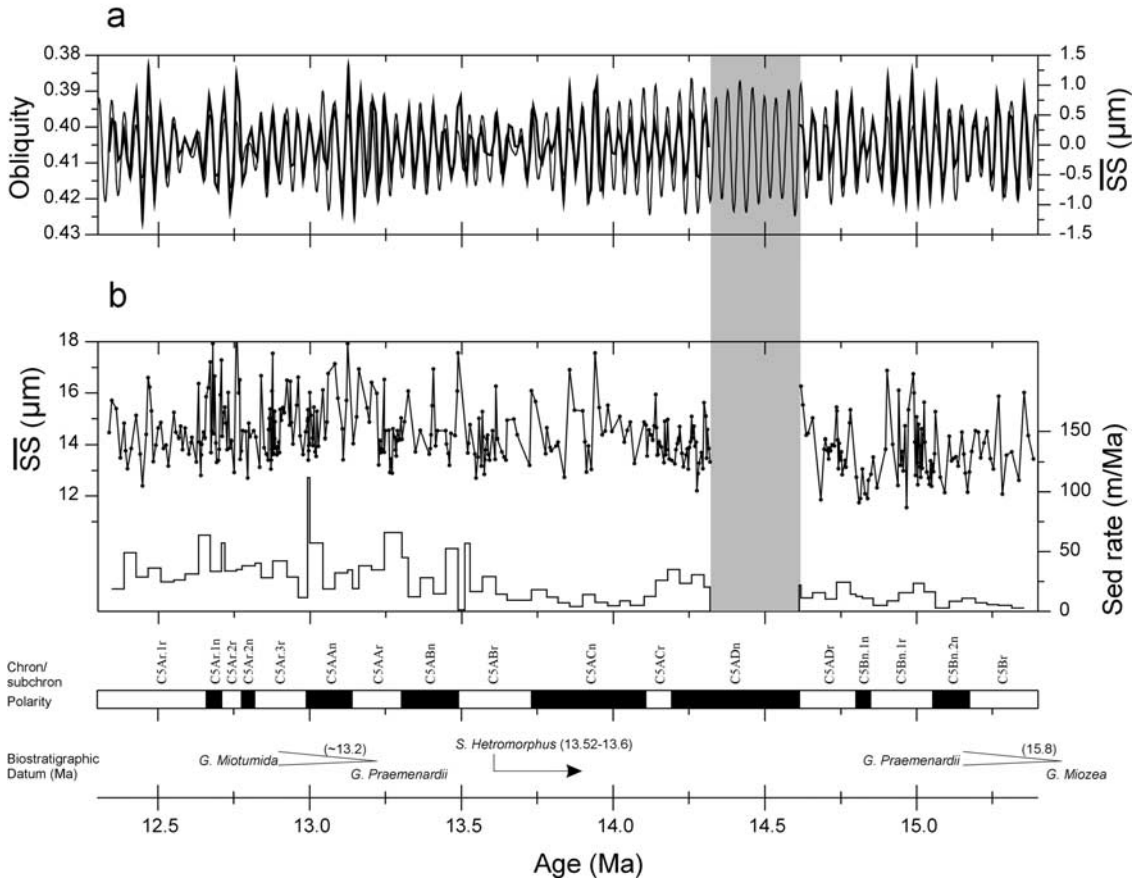

Figure 6. Site 1123 timescale. Shown are (a) comparison of the filtered 41 kyr component of the $\overline{SS}$ with orbital obliquity. The $\overline{SS}$ filter has a central frequency of 0.04065 cycles kyr^{-1} and a bandwidth of 0.01046 cycles kyr^{-1}. (b) The $\overline{SS}$ record versus age together with sedimentation rates. Also shown is the polarity record on the 1123 timescale and biostratigraphic datums [*Carter et al.*, 1999a]. Differences between the GPTS and 1123 timescales are given in Table 1. Shading indicates the time gap at the unconformity. For core recovery, see Figure 3.

associated with orbital obliquity (Figure 5b). The amplitude variations of orbital obliquity and the 41 kyr filter output were then compared (Figure 6). The records are characterized by a remarkable similarity in amplitude modulation between 12.5 and 14.0 Ma and again in the lowermost section between 14.7 and 15.4 Ma. This comparison implies we have adequately mapped the $\overline{SS}$ (as an indirect climate proxy) on to the orbital target. Other variables using the $\overline{SS}$ tuned timescale were examined spectrally for further evidence that the tuning was credible. The calcium carbonate record above the hiatus (Figure 7a) shows a significant spectral peak at the orbital frequency of eccentricity (99.1 kyr at >90% confidence level) but not obliquity. However, a record of Ba/Al measured on mostly the same samples as the $\overline{SS}$, but for a shorter interval, shows a single spectral peak at the frequency of obliquity [*Weedon and Hall*, 2003]. Several small differences exist between the ages of the Chrons shown in Table 1 based on the GPTS [*Berggren et al.*, 1995b] and the Site 1123 timescale presented here. The imperfect nature of the coring record means that the tuning should only be regarded as a working model rather than a contribution toward revision of the GPTS. However, the tuning demonstrates that the cyclic variations in $\overline{SS}$ caused by changes in the flow speed of the DWBC are consistent with an orbital control.

6.2. Long-Term Changes in the Deep Pacific Inflow Speed

[21] Oxygen isotope studies show the middle Miocene (17–15 Ma) climate was warm and typified by low global ice volume, which was followed by a period of significant ice accumulation on Antarctica ~15.6–12 Ma [*Shackleton and Kennett*, 1975; *Kennett*, 1977; *Loutit et al.*, 1983; *Miller and Katz*, 1987; *Miller et al.*, 1991; *Wright et al.*, 1992; *Wright and Miller*, 1993; *Flower and Kennett*, 1993; *Barrett*, 1996]. *Flower and Kennett* [1995] suggest that the middle Miocene EAIS development was controlled by the interplay between SCW and TISW. Their studies of oxygen and carbon isotopes at southwest Pacific DSDP sites [*Flower and Kennett*, 1995] identified three stages in deep ocean circulation associated with EAIS development, in broad agreement with previous studies [*Woodruff and Savin*,

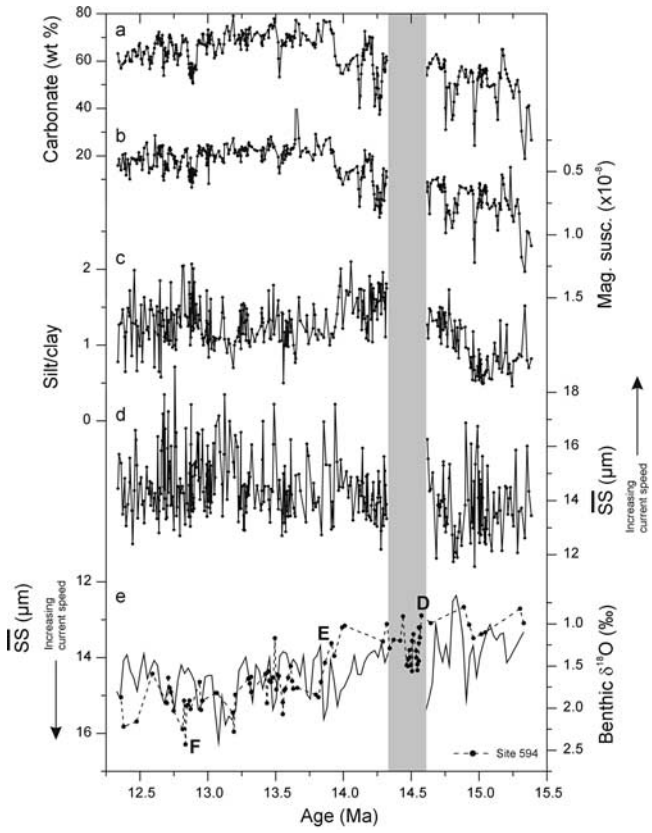

Figure 7. Sedimentological data for Site 1123 versus age. Shown are records of (a) calcium carbonate, (b) magnetic susceptibility (note reversed scale), (c) silt/clay ratio, (d) $\overline{SS}$, and (e) benthic $\delta^{18}O$ record for DSDP Site 594 [*Flower and Kennett*, 1995] together with the $\overline{SS}$ record smoothed to a 25 kyr time step using Gaussian interpolation (note reversed scale). Ages for DSDP Site 594 [*Flower and Kennett*, 1995], based on the timescale of *Cande and Kent* [1992], have been recalibrated to the *Berggren et al.* [1995b] timescale. Stable isotopic events (D, E, F) identified by *Flower and Kennett* [1995] follow the nomenclature of *Woodruff and Savin* [1991].

1989; *Wright et al.*, 1992]. First, the interval between ~16.5–15.6 Ma was characterized by a high-latitude SCW source and some influence of low-latitude, possibly TISW source. Second, a period of deep water circulation dominated by SCW occurred between ~15.6–13.8 Ma. Lastly, the period ~13.8–12 Ma was marked by a further increase in SCW and a strong influx of Pacific Deep Water. *Flower and Kennett* [1995] suggest that the 15.6–13.8 Ma increase in the influence of SCW was associated with high-latitude cooling, but it clearly preceded the major middle Miocene cooling episode between ~14.0 to 13.8 Ma (probably corresponding to Mi3 of *Miller et al.* [1991]). *Wright and Miller* [1996] suggest that SCW was the only source of deep water between ~15–12.5 Ma.

[22] The Site 1123 sedimentological data are shown against age in Figures 7a–7d. For comparison, Figure 7e also shows the benthic $\delta^{18}O$ record from the shallower Site 594 (1204 m water depth; *Flower and Kennett* [1995]), presently at the base of Antarctic Intermediate Water over southern Chatham Rise. The changes in circulation patterns between 15.6 and 12.5 Ma [*Flower and Kennett*, 1995] are in general agreement with the DWBC speed changes suggested by the $\overline{SS}$ current speed proxy. The lowermost section, below the base of the inferred unconformity, is characterized by initially low silt/clay ratios and generally low, but variable, $\overline{SS}$ values. After ~15 Ma silt/clay ratios steadily increase while $\overline{SS}$ values remain variable although they show rapidly increasing values after 14.8 Ma, suggesting increasing flow speeds toward the onset of erosion (or nondeposition) causing the hiatus. The time gap spans distinct $\delta^{18}O$ (and $\delta^{13}C$) maxima centered around 14.5 Ma at Site 594. The latter corresponds to carbon isotopic maximum CM4 of *Woodruff and Savin* [1991]. The unconformity inferred here suggests the presence of vigorous current activity affecting Site 1123 that is broadly coincident with the 14.5 Ma isotopic event. It is believed that this increase in flow speed was driven by thermohaline circulation changes rather than a direct impingement of the ACC north of Chatham Rise (Figure 2). We note that the unconformity coincides with a lithostratigraphic unit boundary at Site 1122 (Bounty Fan, Figure 1) that contains abundant sand and coarse silt interbeds that have been interpreted as contourite deposits [*Carter et al.*, 1999b] suggesting the presence of strong tractive currents to the south (upstream) of, but 1300 m deeper than, Site 1123 (Figure 1).

[23] Increasing flow speeds following the resumption of deposition precede the major middle Miocene cooling at ~14 Ma (Figures 7d and 7e). This cooling event, indicated by the ~1‰ increase in $\delta^{18}O$ at Site 594 (Figure 7e), is characterized by two maxima in flow speed at Site 1123, and coincides with the regional establishment of Neogene benthic assemblages dominated by *E. exigua* [*Kurihara and Kennett*, 1986]. Time-slice reconstruction at 16.3, 13.6 and 12.8 Ma of carbon isotopic values in the southwest Pacific [*Flower and Kennett*, 1995] found that a strong vertical $\delta^{13}C$ gradient in intermediate to deep waters (~3200 m) appeared after 15.6 Ma and increased to a middle Miocene maximum of 0.8 ‰ at 13.6 Ma. *Flower and Kennett* [1995] suggest that southern component intermediate water and Pacific deep water strength were each at a maximum in the southwest Pacific at that time. The increased intermediate water production, affecting Site 594 may have been aided by the paleotopography of the time, including a larger Mernoo Gap (Figure 1.) allowing greater movement of intermediate water northward between the South Island and Chatham Rise. This may have been further aided by there being no Cook Strait at that time. This would have reduced the southward tidal excursion through the Gap, i.e., the prevailing transport would have been north as opposed to now which has the strong south component as well as north [*Heath*, 1985]. The 1123 $\overline{SS}$ record suggests that a period of substantially increased near-bottom current speeds occurred at ~13.2 Ma, centered on a broader general increase in speeds between ~13.6–12.7 Ma (N.B. the down-core maximum is at the hiatus, Figure 7d). Relative speeds recorded in this uppermost section are generally higher than those interpreted from sediments below the 1123 middle Miocene unconformity and

Table 1. Sample, Depth, and Age Comparison Between the GPTS and Site 1123 Age Model for Each Chron Base Within the Middle Miocene Section of 1123

Chron, Base	Core, Section, and Depth, cm	MBSF, m	RMCD, m	Age,[a] Ma	1123 Age, Ma	GPTP-1123 Age, kyr
	181-1123B-					
C5Ar.1r	45X-3, 50	416.10	432.10	12.678	12.659	−19
C5Ar.1n	46X-1, 76	422.96	434.19	12.708	12.710	2
C5Ar.2r	46X-2, 60	424.30	436.61	12.775	12.775	0
C5Ar.2n	46X-2, 145	425.15	438.28	12.819	12.819	0
C5Ar.3r	47X-1, 19	431.99	443.52	12.991	12.989	−2
C5AAn	47X-3, 39	435.19	449.51	13.139	13.140	1
C5AAr	48X-2, 15	443.15	456.77	13.302	13.302	0
C5ABn	48X-3, 66	445.16	462.24	13.510	13.490	−20
C5ABr	49X-2, 30	452.60	466.49	13.703	13.731	28
C5ACn	49X-3, 111	454.91	469.94	14.076	14.108	32
C5ACr	49X-4, 2	456.32	471.83	14.178	14.193	15
C5ADn	50X-2, 29	462.19	475.42	14.612	14.612	0
C5ADr	50X-3, 145	464.85	478.41	14.800	14.800	0
C5Bn.1n	50X-4, 147	465.29	478.97	14.888	14.848	−40
C5Bn.1r	50X-5, 127	467.67	481.70	15.034	15.053	19
C5Bn.2n	51X-1, 29	470.29	482.59	15.155	15.174	19

[a]From *Berggren et al.* [1995b].

are in agreement with the isotopic evidence of increased SCW production in close association with major EAIS growth. The enhanced SCW production is presumably linked to a well-established seasonal freezing of the Antarctic margin [*Kennett and Shackleton*, 1976]. Maximum speeds occurred close to the major isotopic excursions at 12.78 Ma, 13.77 Ma (events E and *F* of *Woodruff and Savin* [1991]), 13.15 Ma and 13.52 Ma. Nonetheless, sedimentological variability at Site 1123 suggests that a Miocene high-resolution isotope record would contain significantly greater variability than is evident in the relatively low-resolution isotopic record from Site 594. *Hall et al.* [2001] suggest that a possible control on the DWBC flow during the Pleistocene is the magnitude of Ekman transport driven by winds at the latitude of Drake Passage [*Toggweiler and Samuels*, 1993]. The modeling studies of *Rahmstorf and England* [1997] concluded that, although such a mechanism has only a moderate influence on the formation of North Atlantic Deep Water the production of AABW depends strongly on the winds over the Southern Ocean. In their experiment a reduction in wind stress from its present level caused a collapse in the Pacific bottom water inflow. We suggest that both the obliquity related variability and the long term increase in the speed of the DWBC during the middle Miocene might be related to increasing wind strength over the Southern Ocean as the atmospheric thermal gradient intensified associated with Antarctic cryosphere expansion.

7. Conclusions

[24] Cyclic variation of middle Miocene $\overline{\text{SS}}$ and lithological records from Site 1123 in the southwest Pacific are dominated by the 41 kyr orbital obliquity cycle. This indicates a strong coupling between the variability in the speed of the DWBC and high-latitude climate forcing. The orbital scale changes in the DWBC flow speed overlay long-term changes that suggest an intensification of the DWBC under an inferred increase in SCW production between ~15.5–12.5 Ma. These results provide evidence that a major component of the deep thermohaline circulation was associated with the middle Miocene growth of the EAIS.

[25] Grain size analyses of sediment material from drift sequences that record the oceanographically relevant $\overline{\text{SS}}$ proxy for near-bottom current speed offer an additional variable for orbital tuning when high-resolution isotopic data are unavailable.

[26] **Acknowledgments.** We thank Anna Fulop for experimental assistance. We are grateful to the two anonymous reviewers for their helpful comments on the manuscript. This research used samples and data provided by the Ocean Drilling Program (ODP), which is sponsored by the U.S. National Science Foundation and participating countries and managed by Joint Oceanographic Institutions Inc. Funding for this research was provided by the Natural Environment Research Council through UK-ODP. IRH gratefully acknowledges support from NIWA's Visiting Scientist Programme.

References

Barrett, P. J., Antarctic paleoenvironment through Cenozoic times—A review, *Terra Antarct.*, *3*, 103–119, 1996.

Berggren, W. A., F. J. Hilgen, C. G. Langereis, D. V. Kent, J. D. Obradovich, I. Raffi, M. E. Raymo, and N. J. Shackleton, Late Neogene chronology: New perspectives in high-resolution stratigraphy, *Geol. Soc. Am. Bull.*, *107*, 1272–1287, 1995a.

Berggren, W. A., D. V. Kent, C. C. Swisher, and M. P. Aubry, A revised Cenozoic geochronology and chronostratigraphy, in *Geochronology, Time Scales and Global Stratigraphic Correlation*, *Spec. Publ., Soc. Econ. Paleontol. Mineral*, vol. 54, edited by W. A. Berggren et al., pp. 129–212, Soc. for Sediment. Geol., Tulsa, Okla., 1995b.

Bianchi, G. G., I. R. Hall, I. N. McCave, and L. Joseph, Measurement of the sortable silt current speed proxy using the Sedigraph 5100 and Coulter Multisizer IIe: Precision and accuracy, *Sedimentology*, *46*, 1001–1014, 1999.

Bianchi, G. G., M. Vautravers, and N. J. Shackleton, Deep flow variability under apparently stable North Atlantic Deep Water production during the last interglacial of the subtropical northwest Atlantic, *Paleoceanography*, *16*, 306–316, 2001.

Cande, S. C., and D. V. Kent, A new geomagnetic polarity timescale for late Cretaceous and Cenozoic, *J. Geophys. Res.*, *97*, 13,917–13,951, 1992.

Cande, S. C., and D. V. Kent, Revised calibration of the geomagnetic polarity timescale for the Late Cretaceous and Cenozoic, *J. Geophys. Res.*, *100*, 6093–6095, 1995.

Carter, L., and I. N. McCave, Development of sediment drifts approaching an active plate margin under the SW Pacific Deep Western Boundary Current, *Paleoceanography*, *9*, 1061–1085, 1994.

Carter, L., and J. Wilkin, Abyssal circulation around New Zealand—A comparison between observations and a global circulation model, *Mar. Geol.*, *159*, 221–239, 1999.

Carter, L., R. M. Carter, I. N. McCave, and J. Gamble, Regional sediment recycling in the abyssal southwest Pacific Ocean, *Geology*, *24*, 735–738, 1996.

Carter, R. M., et al., Site 1123: North Chatham drift—A 20 Ma record of the Pacific Deep Western Boundary Current, *Proc. Ocean Drill. Program Init. Rep.*, *181*, 1–184, 1999a.

Carter, R. M., et al., Site 1122: Turbidites with a contourite foundation, *Proc. Ocean Drill. Program Init. Rep.*, *181*, 1–146, 1999b.

Cullen, D. J., Autochthonous rocks from the Chatham Rise, east of New Zealand, *N. Z. J. Geol. Geophys.*, *8*, 465–474, 1965.

Flower, B. P., and J. P. Kennett, Middle Miocene ocean/climate transition/climate transition: High-resolution stable isotopic records from DSDP Site 588A, southwest Pacific, *Paleoceanography*, *8*, 811–843, 1993.

Flower, B. P., and J. P. Kennett, The middle Miocene climatic transition: East Antarctic ice sheet development, deep ocean circulation and global carbon cycling, *Palaeogeogr. Palaeoclimatol. Palaeoecol.*, *108*, 537–555, 1994.

Flower, B. P., and J. P. Kennett, Middle Miocene deepwater paleoceanography in the southwest Pacific: Relations with East Antarctic Ice Sheet development, *Paleoceanography*, *10*, 1095–1112, 1995.

Gaina, C., D. R. Müller, J.-Y. Royer, J. Stock, J. Hardebeck, and P. Symonds, The tectonic history of the Tasman Sea: A puzzle with 13 pieces, *J Geophys Res.*, *103*, 12,413–12,433, 1998.

Gordon, A. L., The Southern Ocean and global climate, *Oceanus*, *31*, 39–46, 1988.

Hall, I. R., I. N. McCave, M. R. Chapman, and N. J. Shackleton, Coherent deep flow variation in the Iceland and American basins during the last interglacial, *Earth Planet Sci. Lett.*, *64*, 15–21, 1998.

Hall, I. R., I. N. McCave, N. J. Shackleton, G. P. Weedon, and S. E. Harris, Intensified deep Pacific inflow and ventilation in Pleistocene glacial times, *Nature*, *412*, 809–812, 2001.

Hall, I. R., L. Carter, and S. E. Harris, Major depositional events under the deep Pacific inflow, *Geology*, *30*, 487–490, 2002.

Heath, R. A., A review of the physical oceanography of the seas around New Zealand—1982, *N. Z. J. Mar. Freshwater Res.*, *19*, 70–124, 1985.

Hollister, C. D., and I. N. McCave, Sedimentation under deep-sea storms, *Nature*, *309*, 220–225, 1984.

Kennett, J. P., Cenozoic evolution of Antarctic glaciation, the circum-Antarctic ocean and their impact on global paleoceanography, *J. Geophys. Res.*, *82*, 3843–3859, 1977.

Kennett, J. P., and N. J. Shackleton, Oxygen isotopic evidence for the development of the psychrosphere 38 Myr ago, *Nature*, *260*, 513–515, 1976.

Kurihara, K., and J. P. Kennett, Neogene benthic foraminifers: Distribution in depth transverse, *Init. Rep. Deep Sea Drill. Proj.*, *90*, 1037–1078, 1986.

Laskar, J., F. Joutel, and F. Boudin, Orbital, precessional, and insolation quantities for the Earth from -20 Myr to +10 Myr, *Astron. Astrophys.*, *270*, 522–533, 1993.

Ledbetter, M. T., and D. A. Johnson, Increased transport of Antarctic Bottom Water in the Vema Channel during the last Ice Age, *Science*, *194*, 837–839, 1976.

Loutit, T. S., J. P. Kennett, and S. M. Savin, Miocene equatorial and southwest Pacific paleoceanography from stable isotope evidence, *Mar. Micropaleontol.*, *8*, 215–233, 1983.

Mann, M. E., and J. Lees, Robust estimation of background noise and signal detection in climatic time series, *Clim. Change*, *33*, 409–445, 1996.

Marcantonio, F., R. F. Anderson, S. Higgins, P. Schlosser, and P. Kubik, Sediment focusing in the central equatorial Pacific Ocean, *Paleoceanography*, *16*, 260–267, 2001.

McCave, I. N., Erosion, transport and deposition of fine grained marine sediments, *Geol. Soc. London Spec. Publ.*, *15*, 35–69, 1984.

McCave, I. N., and L. Carter, Recent sedimentation beneath the Deep Western Boundary Current off northern New Zealand, *Deep Sea Res.*, *44*, 1203–1237, 1997.

McCave, I. N., B. Manighetti, and S. G. Robinson, Sortable silt and fine sediment size/composition slicing: Parameters for paleocurrent speed and paleoceanography, *Paleoceanography*, *10*, 593–610, 1995.

Miller, K. G., and M. E. Katz, Oligocene to Miocene benthic foraminiferal and abyssal circulation changes in the North Atlantic, *Micropaleontology*, *33*, 97–149, 1987.

Miller, K. G., J. D. Wright, and R. G. Fairbanks, Unlocking the icehouse: Oligocene-Miocene oxygen isotope eustacy and margin erosion, *J. Geophys. Res.*, *96*, 6829–6848, 1991.

Morgans, H. E. G., G. H. Scott, A. G. Beu, I. J. Graham, T. C. Mumme, W. St. George, and C. P. Strong, New Zealand Cenozoic time scale (version 11/96), *Rep. Inst. Geol. Nucl. Sci.*, *96/38*, 1–12, 1996.

Morrow, R. A., J. A. Church, R. Coleman, D. B. Chelton, and N. White, Eddy momentum flux and its contribution to the Southern Ocean momentum balance, *Nature*, *357*, 482–484, 1992.

Nelson, C. S., C. H. Hendy, A. M. Cuthbertson, and G. R. Jarrett, Late Quaternary carbonate and isotope stratigraphy, subantarctic Site 594, southwest Pacific, *Init. Rep. Deep Sea Drill. Proj.*, *90*, 1425–1436, 1986.

Orsi, A. H., G. C. Johnson, and J. L. Bullister, Circulation, mixing, and production of Antarctic Bottom Water, *Progr. Oceanogr.*, *43*, 55–109, 1999.

Paillard, D., L. Labeyrie, and P. Yiou, Macintosh program performs time-series analysis, *Eos Trans. AGU*, *77*, 379, 1996.

Press, W. H., S. A. Teukolsky, W. T. Vetterling, and B. P. Flannery, *Numerical Recipes, the Art of Scientific Computing*, 2nd ed., Cambridge Univ. Press, New York, 1992.

Rahmstorf, S., and M. H. England, Influence of Southern Hemisphere winds on North Atlantic Deep Water flow, *J. Phys. Oceanogr.*, *27*, 2040–2054, 1997.

Ramsay, A. T. S., C. W. Smart, and J. C. Zachos, A model of early middle Miocene deep ocean circulation for the Atlantic and Indian Oceans, *Geol. Soc. London Spec. Publ.*, *131*, 55–77, 1998.

Schmitz, W. J., On the interbasin-scale thermohaline circulation, *Rev. Geophys.*, *33*, 151–173, 1995.

Sclater, J., L. Meinke, A. Bennett, and C. Murphy, The depth of the ocean through the Neogene, *Mem. Geol. Soc. Am.*, *163*, 1–19, 1985.

Scott, G. H., The late Miocene to early Pliocene history of the *Globorotalia miozea* plexus from Blind River, New Zealand, *Mar. Micropalentol.*, *4*, 341–361, 1979.

Shackleton, N. J., and J. P. Kennett, Paleotemperature history of the Cenozoic and the initiation of Antarctic glaciation: Oxygen and carbon isotope analyses in DSDP sites 277, 279 and 281, *Init. Rep. Deep Sea Drill. Proj.*, *29*, 143–156, 1975.

Stickley, C. E., L. Carter, I. N. McCave, and P. P. E. Weaver, Variations in the CDW flow through the SW Pacific gateway for the last 190 ky: Evidence from Antarctic diatoms, in *The Oceans and Rapid Climate Change: Past, Present, and Future*, *Geophys. Monogr.*, vol. 126, edited by D. Seidov et al., pp. 101–116, AGU, Washington, D.C., 2001.

Stommel, H., The abyssal circulation, *Deep Sea Res.*, *5*, 80–82, 1958.

Sykes, T. J. S., A. T. S. Ramsay, and R. B. Kidd, Southern Hemisphere Miocene bottom-water circulation: A palaeobathymetric analysis, *Geol. Soc. London Spec. Publ.*, *131*, 14–54, 1998.

Syvitski, J. P. M., (Ed.), *Principles, Methods and Application of Particle Size Analysis*, 368 pp., Cambridge Univ. Press, New York, 1991.

Toggweiler, J. R., and B. Samuels, Is the magnitude of the deep outflow from the Atlantic Ocean actually governed by Southern Hemisphere winds?, in *The Global Carbon Cycle*, edited by H. Heimann, pp. 333–366, Springer-Verlag, New York, 1993.

Warren, B. A., Transpacific hydrographic sections at lats. 43°S and 28°S, the SCORPIO expedition, II: Deep water, *Deep Sea Res.*, *20*, 9–38, 1973.

Warren, B. A., Deep circulation of the world ocean, in *Evolution of Physical Oceanography*, edited by B. A. Warren and C. Wunsch, pp. 6–41, MIT Press, Cambridge, Mass., 1981.

Weaver, P. P. E., H. L. Neil, and L. Carter, Sea surface temperature estimates from the Southwest Pacific based on planktonic foraminifera and oxygen isotopes, *Palaeogeogr. Palaeoclimatol. Palaeoecol.*, *131*, 241–256, 1997.

Weedon, G. P., and I. R. Hall, Neogene palaeoceanography of Chatham Rise (S.W Pacific) based on sediment geochemistry, *Mar. Geol*, in press, 2003.

Whitworth, T., B. A. Warren, W. D. Nowlin, R. D. Pillsbury, and M. L. Moore, On the deep western-boundary current in the southwest Pacific Basin, *Prog. Oceanogr.*, *43*, 1–54, 1999.

Woodruff, F., and S. Savin, Miocene deepwater oceanography, *Paleoceanography*, *4*, 87–140, 1989.

Woodruff, F., and S. Savin, Mid-Miocene isotope stratigraphy in the deep sea: High-resolution correlations, paleoclimatic cycles, and sediment preservation, *Paleoceanography*, *6*, 775–806, 1991.

Wright, J. D., and K. G. Miller, Southern Ocean influences on Eocene to Miocene deepwater circulation, *Antarct. Res. Ser.*, *60*, 1–25, 1993.

Wright, J. D., and K. G. Miller, Control on North Atlantic deep water circulation by the Greenland-Scotland Ridge, *Paleoceanography*, *11*, 157–170, 1996.

Wright, J. D., K. G. Miller, and R. G. Fairbanks, Early and middle Miocene stable isotopes: Implications for deepwater circulation and Climate, *Paleoceanography*, *7*, 357–389, 1992.

L. Carter, National Institute of Water and Atmosphere, PO Box 14 901, Kilbirnie, Wellington, New Zealand. (l.carter@niwa.cri.nz)

I. R. Hall, Department of Earth Sciences, Cardiff University, PO Box 914, Cardiff CF10 3YE, UK. (Hall@cardiff.ac.uk)

P. C. Knutz, Geological Institute, University of Copenhagen, Øster Voldgade 10, DK-1350 Copenhagen, Denmark. (knutz@geo.geol.ku.dk)

I. N. McCave, Department of Earth Sciences, University of Cambridge, Downing Street, Cambridge CB2 3EQ, UK. (McCave@esc.cam.ac.uk)

G. P. Weedon, Centre for Environmental Change and Volcanic Studies, University of Luton, Park Square, Luton LU1 3JU, UK. (graham.weedon@luton.ac.uk)

R. Zahn, Institució Catalana de Recerca i Estudis Avançats, ICREA, GRC Geociències Marines, Facultat de Geologia, Universitat de Barcelona, Campus de Pedralbes, E-08028 Barcelona, Spain. (Rainer@geo.ub.es)